A&A 545, A143 (2012)
DOI: 10.1051/0004-6361/201219561

Astronomy & Astrophysics

Extended soft X-ray emission in 3CR radio galaxies at $z < 0.3$: high excitation and broad line galaxies⋆

B. Balmaverde[1], A. Capetti[1], P. Grandi[2], E. Torresi[2], M. Chiaberge[3,4,5], J. Rodriguez Zaurin[6], G. R. Tremblay[7], D. J. Axon[8,9], S. A. Baum[10,11], G. Giovannini[3,12], P. Kharb[8], F. D. Macchetto[4], C. P. O'Dea[8,13], and W. Sparks[4]

[1] INAF – Osservatorio Astrofisico di Torino, Strada Osservatorio 20, 10025 Pino Torinese, Italy
e-mail: balmaverde@oato.inaf.it
[2] INAF – IASF – Istituto di Astrofisica e Fisica cosmica di Bologna, via P. Gobetti 101, 40129 Bologna, Italy
[3] INAF – Istituto di Radioastronomia di Bologna, via Gobetti 101, 40129 Bologna, Italy
[4] Space Telescope Science Institute, 3700 San Martin Drive, Baltimore, MD 21218, USA
[5] Center for Astrophysical Sciences, Johns Hopkins University, 3400 N. Charles Street Baltimore, MD 21218, USA
[6] Instituto de Astrofísica de Canarias, Calle vía Láctea s/n, 38205 La Laguna, Tenerife, Spain
[7] European Southern Observatory, Karl-Schwarzschild-Str. 2, 85748 Garching bei Muenchen, Germany
[8] Dept of Physics, Rochester Institute of Technology, 84 Lomb Memorial Dr., Rochester, NY 14623, USA
[9] School of Mathematical and Physical Sciences, University of Sussex, Falmer, Brighton, BN2 9BH, UK
[10] Carlson Center for Imaging Science, 84 Lomb Memorial Dr., Rochester, NY 14623, USA
[11] Radcliffe Institute for Advanced Study, 10 Garden St. Cambridge, MA 02138, USA
[12] Dipartimento di Astronomia, Universitá di Bologna, via Ranzani 1, 40127 Bologna, Italy
[13] Harvard Smithsonian Center for Astrophysics, 60 Garden St. Cambridge, MA 02138, USA

Received 8 May 2012 / Accepted 1 August 2012

ABSTRACT

We analyze *Chandra* observations of diffuse soft X-ray emission associated with a complete sample of 3CR radio galaxies at $z < 0.3$. We focus on the properties of the spectroscopic sub-classes of high excitation galaxies (HEGs) and broad line objects (BLOs). Among the 33 HEGs we detect extended (or possibly extended) emission in about 40% of the sources; the fraction is even higher (8/10) when restricting the analysis to the objects with exposure times larger than 10 ks. In the 18 BLOs, extended emission is seen only in two objects; this lower detection rate can be ascribed to the presence of their bright X-ray nuclei that easily outshine any genuine diffuse emission. A very close correspondence between the soft X-ray and optical line morphology emerges. We also find that the ratio between [O III] and extended soft X-ray luminosity is confined within a factor of 2 around a median value of 5. Both results are similar to what is seen in Seyfert galaxies. We discuss different processes that could explain the soft X-ray emission and conclude that the photoionization of extended gas, coincident with the narrow line region, is the favored mechanism.

Key words. galaxies: active – X-rays: galaxies – ISM: jets and outflows

1. Introduction

Supermassive black holes (SMBHs) have a profound effect on the evolution of galaxies but the nature of the relationship between these two entities is still an open problem. This depends on how much of the released energy interacts with the surrounding matter and how this accretes onto the SMBHs. This feedback process can be explored through a multi-wavelength analysis of the emission observed in the circumnuclear regions. The vast collection of emission lines, ranging from the mm to the X-ray bands, reveal the presence of a complex multiphase medium surrounding the active galactic nucleus (AGN). Of special interest for our purposes is the so-called narrow line region (NLR) where optical emission lines with widths of several hundreds of km s^{-1} are produced. The NLR is just outside (or even within) the SMBHs sphere of influence and its physical and dynamical properties are strongly affected by the central engine. It exists at the interface between the active nucleus and the galaxy, and is thus a convenient laboratory in which to explore the energy exchange between the two. Moreover, the NLR is mostly free from the effects of obscuration and it is resolved in most nearby AGN, allowing us to perform spatially resolved studies and morphological comparisons in different energy bands. Indeed, it offers a wide variety of diagnostic tools to probe the gas physical conditions.

The NLR and the processes that occur in it have been extensively studied in many bands. In this paper we focus our study on the properties of the circumnuclear emission seen in the *Chandra* soft X-ray images in the complete sub-sample of nearby ($z < 0.3$) 3CR radio galaxies with high excitation (HEGs) or broad (BLO) emission lines.

The first case reported in the literature of extended soft X-ray emission (below ∼2 keV) associated with an AGN is the Seyfert galaxy NGC4151 (Elvis et al. 1983) observed with *Einstein*. Since then, it has been recognized that a few bright, nearby Seyfert 2 galaxies are associated with soft X-ray emission extending over ∼1 kpc and matching very closely the morphology of the optical NLR (e.g., Elvis et al. 1990). This result was strengthened by later observations by the *Einstein* and ROSAT satellites (e.g., NGC 1068: Wilson et al. 1992; NGC 2992: Elvis et al. 1990; NGC 2110: Weaver et al. 1995). This was not a

⋆ Appendix A is available in electronic form at http://www.aanda.org

totally unexpected result, because a hot medium in pressure equilibrium with the NLR is thought to be necessary to prevent the optical emitting line clouds from evaporating (Krolik & Vrtilek 1984). In fact initially the preferred explanation of these extended soft X-ray regions was an outflow of hot, collisionally ionized gas, that confines the narrow-line clouds (Wilson et al. 1992; Elvis et al. 1990; Weaver et al. 1995), although other emission mechanisms, such as scattering of nuclear light, could not be ruled out.

Recently, with the advent of a new generation of higher resolution and sensitivity X-ray telescopes, such as *Chandra* and *XMM-Newton*, more detailed comparison on sub-arcsec scales between the X-ray, optical, and radio emission has been possible. *Chandra* images at high resolution and XMM spectroscopic observations, combined with *Hubble* Space Telescope (HST) and VLA images, have been used to investigate a larger number of bright, nearby AGN, mostly Seyfert galaxies (e.g., NGC 2110 Evans et al. 2006). Bianchi et al. (2006) studied a sample of 8 Seyferts and found extended soft X-ray emission co-spatial with the NLR for all of their sources. High resolution spectroscopic observations of the extended X-ray emitting regions performed with *Chandra*/HETGS, possible in a few cases (e.g. NGC 1068 Ogle et al. 2003; NGC 4151 Wang et al. 2011) reveals that the soft X-ray part of the spectrum is dominated by emission lines mainly from He- and H-like K transitions of light metals similar to those observed in their nuclei (e.g. MRK 3: Sako et al. 2000; Circinus: Sambruna et al. 2001a). X-ray observations made with the Reflection Grating Spectrometers (RGS) onboard *XMM-Newton* have lower resolution (15″), thus encompassing both the nucleus and the soft X-ray extended region. The resulting spectra therefore represent intensity-weighted conditions over kpc scales, but they are consistent with an ensemble of several narrow emission lines (e.g. Kinkhabwala et al. 2002; Guainazzi & Bianchi 2007; NGC 5252: Dadina et al. 2010).

Nevertheless, although in Seyfert 2 galaxies the most probable explanation is that the gas is photoionized by the AGN, there is no general consensus about the dominant process that produces the soft X-ray extended emission in other classes of galaxies. In fact, a variety of different mechanisms could be considered, such as: a hot component of a multiphase interstellar medium, hot gas shocked and evacuated by an outflow or a jet, or an outflow of collisionally ionized gas escaping from the nucleus, driven by radiation, that interacts with the NLR clouds. In an outflow model, the NLR kinematics are dominated by radiation and/or wind pressure driving clouds outwards from the nucleus (Crenshaw et al. 2000) and indeed complex motions in the NLR are often inferred.

The literature on the X-ray properties of the NLR in radio galaxies is more limited than for Seyferts. At high energies (between 2 and 10 keV) radio galaxies show a compact nuclear component and, in some cases, collimated structures co-spatial with the radio emission. Only recently extended regions in soft X-rays, similar to that observed in Seyfert galaxies, have been discovered (e.g., in 3C 171: Hardcastle et al. 2010; 3C 33: Torresi et al. 2009; 3C 305: Massaro et al. 2009; Hardcastle et al. 2012; and PKS 1138-262: Carilli et al. 2002). In all cases the soft X-ray emitting regions are closely spatially related to the optical emission lines, similar to what is observed for radio quiet AGN. Also, analysis of the nuclei performed with high or medium resolution spectroscopic data reveals many emission lines in the soft band, as observed in the radio-quiet AGN (e.g. 3C 445: Sambruna et al. 2007; Grandi et al. 2007; 3C 33: Torresi et al. 2009; 3C 234: Piconcelli et al. 2008).

In this work we perform a complete analysis of the properties of X-ray emission in the soft band (0.5–2 keV) for 113 3CR radio galaxies at $z < 0.3$ (from Spinrad et al. 1985). A *Chandra* snapshot survey has been recently completed to provide us with observations of all 3CR sources not already covered by other programs. Now we can take advantage of a complete database of high resolution X-ray observations. In this paper we focus on the extended circumnuclear emission of the galaxies classified as HEG and BLO. Our aim is to establish whether extended emission is present, and to explore the relationship with the overall multi-band properties of the galaxy.

The multi-wavelength data we will use are mainly from the ground based spectroscopic survey presented by Buttiglione et al. (2009, 2010, 2011), leading to a classification into the three main classes: broad line objects (BLO), low and high excitation galaxies (LEG and HEG). Furthermore, emission line imaging surveys of the 3CR sources have been carried out using both ground-based telescopes (McCarthy et al. 1995; Baum et al. 1988) and HST (Privon et al. 2008; Tremblay et al. 2009).

We adopted the following cosmological parameters: $H_0 = 71\ \mathrm{km\,s^{-1}\ Mpc^{-1}}$, $\Omega_\mathrm{M} = 0.27$, $\Omega_\Lambda = 0.73$ (Spergel et al. 2003).

2. The sample and the observations

The sample of 3CR radio galaxies at redshift $z < 0.3$ has been entirely observed by *Chandra*. In particular we consider the 113 3CR sources from Spinrad et al. (1985) with $z < 0.3$ (having only excluded 3C 231, aka M 82, a star burst galaxy and 3C 71, aka NGC 1068, a Seyfert galaxy). The sample includes a significant number of powerful classical edge-brightened FR II radio galaxies, as well as the more common (at low redshift) edge-darkened FR Is (Fanaroff & Riley 1974). In this paper we focus on the 51 objects classified as HEGs or BLOs in Buttiglione et al. (2010, 2011). We include these two classes in our study because their differences can be ascribed only to selective nuclear obscuration and they are likely to differ only by their orientation with respect to our line of sight (e.g., Antonucci 1993). Indeed, although the HEGs and BLOs differ in the presence of the broad component of the permitted lines, the luminosities and ratios of the narrow emission lines are indistinguishable.

We downloaded from the *Chandra* archive the observations for all HEG and BLO sources. The *Chandra* Obs. ID and exposure times for the 51 sources of our sample are listed in Table 1. Most of these data sets (31) were obtained as part of a two cycle snapshot proposal (PI Dan Harris, exposure time 8 ks per target).

We applied the standard reduction data procedure using the *Chandra* Interactive Analysis of Observations CIAO 4.3, with *Chandra* Calibration Database CALDB version 4.4.1. We set the observation specific bad pixel files and when necessary we filtered data to remove flares, then we generated a new level = 2 event file, using the chandra_repro reprocessing script. The standard grade, status, and good time filters were applied.

3. Imaging analysis

As the aim of this paper is the study of the extended soft X-ray emission, we need a quantitative method to establish when such a structure is indeed present in addition to the nuclear point source. In order to define a source as "extended", we compare its surface brightness profile (SBP) with that of the theoretical point spread function (PSF).

The *Chandra* PSF depends on both the incident spectrum and on the source location. We produce the appropriate PSF

utilizing *Chandra* PSF simulator (ChaRT) for each individual source. The input parameters of this software are the position of the observed source on the detector (the off-axis and the azimuthal angle), the exposure time, and the model spectrum. The model spectrum is obtained from a fit to the point source emission. The result of the simulation are a collection of rays that MARX projects onto the detector plane obtaining a pseudo-event file that can be directly compared with the observations.

We then obtain the SBP of each source by measuring the net counts in a series of equally spaced annuli centered on the nucleus, with a step of 1 pixel, and dividing by the respective areas. We normalize the PSF to match the observed SBP in the first 2 pixels and we look for an excess in the bins at larger radii. In the case of sources affected by pile-up the normalization is instead performed in an annulus of radius between 3 and 5 pixels. We consider a source as "extended" when we measure an excess of the SBP with respect to the PSF with a significance greater than 3σ. We instead classify a source as "possibly extended" when we derive an excess at a significance level between 2σ and 3σ. The objects that do not show any evidence of extended features, were classified as "non extended" objects or "non detected" if no emission is present at all.

However, the SBP method is not always well suited to capturing the presence of the faint, elongated structures we often see in our images. We therefore considered a second criterion. In order to emphasize the departure from circular symmetry of any extended emission we compare the counts in two rectangular boxes, one aligned with the axis of optical NLR (or eventually along the radio axis) and the second box orthogonal to the first one. The central square formed by the intersection of the two boxes, which contains the nuclear source, is excluded from analysis. We consider as "extended" (or "possibly extended") the sources in which the difference between the counts in the two boxes have a significance larger than 3σ (or between 2 and 3σ). The reduced uncertainty, associated with the lower background and PSF contribution due to the smaller integration areas, corresponds to a higher number of objects with a positive detection of extended emission with this latter method.

This classification is reported in Table 1. Soft X-ray images of the "extended" and "possibly extended" sources are shown in Fig. 1.

The CIAO tool *srcextent* is commonly used to measure the size and the position angle (PA) of X-ray emission (see Table 1). However, this measurement is dominated by the structure of the nuclear source and it does not return satisfactory measurements for our sources because we are instead interested in the properties of the extended emission alone. We therefore measured the source extension and the PA inspecting the iso-counts contours. In Table 1 we also provide a short additional description of the soft X-ray morphology for a few cases of interest.

4. Flux measurements

We extract the spectrum of the "extended" and "possibly extended" sources shown in Fig. 1. The spectral extraction region is formed by one or two rectangular boxes, whose position has been chosen based on the X-ray morphology, or, in a few cases, also the NLR morphology. To avoid nuclear contamination we position the inner boundary of the boxes at a distance of at least 1.″2 or 1.″5 from the nucleus, depending on its brightness.

In 5 sources (namely 3C 171, 3C 305, 3C 403, 3C 433, and 3C 445) the number of counts in the soft band (between 51 and 134) are sufficient to perform a spectral analysis. We re-bin the spectra with at least 10 counts/bin and apply the Poissonian Cash statistic (except for 3C 171 and 3C 445, for which we re-bin the spectrum at 20 counts/bin and use the χ^2 statistic). We consider three models to fit the entire energy range: power-law, MEKAL[1], and XSTAR (Bautista & Kallman 2001). As discussed in more detail below, these models correspond to three different radiation mechanisms in which the soft X-ray emission can be ascribed to i) scattered nuclear X-ray light from free electrons; ii) hot gas that is collisionally ionized; and iii) photoionized gas clouds.

In addition to the dominant soft X-ray emission, we note the presence of a high energy bump (above $\gtrsim$2–3 keV) in all sources for which spectral analysis was possible (except for 3C 305). As discussed below, this can be ascribed to the leaking of the nuclear emission due to the larger PSF extent at higher energies.

As an example, we show in Fig. 3 the spectrum of 3C 403 fitted with the 3 different models. In addition to the extended component, we added an intrinsically absorbed power law to reproduce the emission above 2 keV. Using simulated PSFs from ChaRT and MARX, we confirmed that although the absorbed nucleus in 3C 403 contributes only ~0.3% of the extended flux in the 0.5–2 keV range, it can produce substantial leakage at higher energy. For this source, the predicted flux value in the extended region of the galaxy is consistent with the value of ~2%, obtained from the spectral fit. The fit for the other 4 sources are given in the appendix. The fit results are given in Table 2 and will be discussed in Sect. 7.

Apart from these five sources, the observed counts in the extended regions are not sufficient for a detailed spectral analysis. Nonetheless, as discussed below, a robust conversion between counts and fluxes can be still obtained.

We convert the measured counts into X-ray fluxes adopting the same models used above. For each model the normalization is set in order to match the model count rate to the observed one. We correct the observed fluxes of each source for the Galactic column density as given by XSPEC and report them in Table 3. For the power-law model we used as reference value for the photon index $\Gamma = 1.7$. For MEKAL model we fixed the temperature at $kT = 1$ keV, the abundance at 0.5 of the solar value, the hydrogen density at 1 cm^{-3}. For the XSTAR model, we generate a table with XSTAR2XSPEC that can be used in the model fitting data by XSPEC. The electron gas density of the clouds is held constant to $N_e = 10^3$ cm^{-3} and the temperature is fixed to $T = 10^5$ K. We choose as input configuration a simple photoionization model comprising a power-law continuum, $f_\nu \propto \nu^\alpha$ ($\alpha = -0.7$ fixed), that is photo-ionizing optically thick, solar abundance emitting clouds.

Different models do not produce relevant discrepancies on the resulting flux values: for a power-law, a collisional hot diffuse gas, or a photo-ionized gas, we obtain marginal flux differences usually within a ±10% level (see Table 3).

We also explore how our choice of the model parameters affects the flux measurements. We choose an arbitrary source test (we verified that it is observed near the aim-point in ACIS/S; the result that we obtain can be extended to all the sources observed near this position on the detector). We calculated the model flux for different combinations of the varying parameters with respect to the reference value and we plot these ratios in Fig. 4. For the power-law model we used as reference value for the photon index $\Gamma = 1.7$, and explored the range $\Gamma = 1.4$–2.0. For MEKAL model we varied the temperature in the range $kT = 0.1$–2 keV. For the XSTAR model, we varied two parameters: the ionization

[1] We also considered an apec model, but the results are indistinguishable from those obtained with MEKAL and are not reported.

Table 1. Radio, soft X-ray and optical emission line properties for HEG and BLO objects of the sample.

Name	Redshift	Classif.	Radio properties			SoftX properties						Opt. lines properties				Host PA
		FR/spec	Size	PA	Ref.	ObsId.	Exp.	Off angle	morph.	Size	PA	morph.	Size	PA	Ref.	
			(″)	(°)			(ks)	(′)		(″)	(°)		(″)	(°)		(°)
(1)	(2)	(3)	(4)	(5)	(6)	(7)	(8)	(9)	(10)	(11)	(12)	(13)	(14)	(15)	(16)	(17)
3C 020	0.174	2/HEG	51	101	3	9294	8	0.3	non det							130
3C 033	0.0596	2/HEG	270	19.2	4	6910	20	1.8	ext	6.9	51	ext		65	3	148[a]
3C 061.1	0.184	2/HEG	186	2	3	9297	8	0.5	unres							165
3C 063	0.175	HEG	22	34	1	12722	8	0.3	ext	11.8	55	ext(unres)		74	3	79
3C 079	0.2559	2/HEG	86	105	3	12723	8	0.3	unres			ext		146	3	71
3C 093.1	0.2430	HEG	0.3	165	1	12725	8	0.3	unres			part.res.		65	1	132
3C 098	0.0304	2/HEG	314	21	2	10234	30	0.5	ext	13	21	ext		148	3	55[b]
3C 105	0.089	2/HEG				9299	8	3.0	unres							
3C 133	0.2775	2/HEG	12	107	3	9300	8	0.3	unres							87
3C 135	0.1253	2/HEG	130	70	1	9301	8	0.3	unres			ext(part.res.)	3.71	54	1	141
3C 136.1	0.064	2/HEG	522	108	1	9326	10	0.3	unres			part.res.	0.53	175	1	117[b]
3C 171	0.2384	2/HEG	30	99	1	10303	60	0.2	ext	17	97	ext	3.44	85	1	66
3C 180	0.22	2/HEG			3	12728	8	0.3	poss.ext	3.0	50	ext		26	3	28
3C 192	0.0598	2/HEG	192	124	1	9270	10	0.3	unres			non det(ext)		161	3	
3C 223	0.1368	2/HEG	300	164	1	12731	8	0.2	unres			ext	2.1	128	1	93
3C 223.1	0.107	2/HEG	117	15	3	9308	8	0.3	unres							40
3C 234	0.1848	2/HEG	110	64	1	12732	8	0.3	poss.ext	5.0	64	ext	2.37	79	1	80
3C 277.3	0.0857	2/HEG	29	158	1	11391	25	0.3	blobby			part.res.		147	3	170[b]
3C 284	0.2394	2/HEG	176	101	1	12735	8	0.3	unres			ext(unr)	2.9	74	1	151
3C 285	0.0794	2/HEG		82.8	4	6911	40	1.0	unres			ext		81	3	129[a]
3C 300	0.27	2/HEG	96	130	3	9311	8	0.3	unres			ext		126,90	3	89
3C 303.1	0.267	2/HEG	1.9	130	1	9312	8	0.3	unres			ext	1.56	140	1	169
3C 305	0.0416	2/HEG	14	44	1	9330	8	0.3	ext	7.3	54	ext	6.37	46	1	76[b]
3C 321	0.096	2/HEG	309	131	1	3138	50	0.8	complex			ext	6.21	108	1	
3C 327	0.1041	2/HEG	169	100	3	6841	40	1.7	unres			ext		22	3	135
3C 379.1	0.256	2/HEG	76	161	1	12739	8	0.3	poss.ext	2.1	40	ext	0.72	43	1	
3C 381	0.1605	2/HEG	69	4	1	9317	8	0.3	unres			ext	5.69	150	1	156
3C 403	0.0590	2/HEG	230	79	2	2968	50	0.5	ext	6.6	34			23	3	39[b]
3C 433	0.1016	HEG	58	172	1	7881	40	0.5	ext	6.5,10.3	138,49	part.res.	5.87	135	1	145[a]
3C 436	0.2145	2/HEG	105	172	1	9318	8	0.3	unres			part.res.			1	3
3C 452	0.0811	2/HEG	277	79	1	2195	80	2.2	ext	6.9	48	part.res.	1.58	125	1	101[b]
3C 456	0.2330	2/HEG	10	20	3	12746	8	0.3	ext	6.1	20					107
3C 458	0.2890	HEG	161	75	1	12747	8	0.3	non det			part.res.(ext)		75	1	
3C 017	0.2198	2/BLO	30	147	1	9292	8	0.3	unres			part.res.		41	1	42
3C 018	0.188	2/BLO				9293	8	0.3	unres							
3C 033.1	0.1809	2/BLO	216	45	3	9295	8	0.3	unres			ext		53	3	63
3C 111	0.0485	2/BLO	220	62	1	9279	10	0.3	unres			non det			1	22[b]
3C 184.1	0.1182	2/BLO	167	157	1	9305	8	0.3	unres			part.res.	2.64	24	1	40
3C 197.1	0.1301	2/BLO	14	2	3	9360	8	0.3	unres			unres			2	
3C 219	0.1744	2/BLO	184	40	1	827	20	0.6	unres			unres			1	145
3C 227	0.0861	2/BLO	246	86	1	6842	30	1.7	unres			ext(unr)		35,119	3	165[b]
3C 273	0.1583	BLO				4879	40	1.1	unres			ext(no bg)			1	
3C 287.1	0.2159	2/BLO	112	91	3	9309	8	0.3	unres							142
3C 303	0.141	2/BLO	38	97	3	1623	15	0.6	unres							0[a]
3C 323.1	0.264	2/BLO				9314	8	0.3	unres			ext(no bg)			1	
3C 332	0.1517	2/BLO	81	20	1	9315	8	0.3	unres			unres			1	54
3C 382	0.0578	2/BLO	179	50	1	4910	55	0.1	unres			part.res.(ext)	2.14	112	1	85[b]

Table 1. continued.

Name	Redshift	Classif.	Radio properties				SoftX properties				Opt. lines properties				Host PA
		FR/spec	Size	PA	Ref.	ObsId.	Exp.	Off angle	morph.	Size	PA	morph.	Size	PA	Ref.	
			(″)	(°)			(ks)	(′)		(″)	(°)		(″)	(°)		(°)
(1)	(2)	(3)	(4)	(5)	(6)	(7)	(8)	(9)	(10)	(11)	(12)	(13)	(14)	(15)	(16)	(17)
3C 390.3	0.0561	2/BLO	231	145	1	830	35	2.3	unres			part.res.	0	62	1	82[b]
3C 410	0.2485	BLO	13	129	3	12742	8	0.3	unres						10	
3C 445	0.0562	2/BLO	576	171	1	7869	50	3.7	ext	14	44	ext(non det)		37	3	80[b]
3C 459	0.2199	2/BLO	8	94	3	12734	8	0.2	ext		102					160

Notes. Column description: (Col. 1) 3CR name; (Col. 2) redshift from Spinrad et al. (1985); (Col. 3) morphological FR type from Buttiglione et al. (2009) and spectroscopic classification into High Excitation Galaxy (HEG) or Broad Line Object (BLO) from Buttiglione et al. (2009). Except for 3C 433 and 3C 458, all the unclassified objects could be considered FR II according to their morphology and 178 MHz luminosities. (Col. 4) Angular size of the radio emission in arcsec; (Col. 5) position angle of the radio source, generally measured from hot spot to hot spot. (Col. 6) References for the radio properties: 1.) Privon et al. (2008), 2.) Martel et al. (1999), 3.) de Koff et al. (1996), 4.) Saripalli & Subrahmanyan (2009); (Col. 7) *Chandra* observation identification number; (Col. 8) approved exposure time for the observation in ks. (Col. 9) off-axis angle coordinate in arcmin. (Col. 10) morphology of the soft (0.5–2 keV) X-ray emission: extended (ext), possibly extended (poss. ext), unresolved (unres), non detected (non det). X-ray jets have been seen in 3C 15: Kataoka et al. (2003), 3C 31: Hardcastle et al. (2002), 3C 66B: Hardcastle et al. (2001), 3C 78: Massaro et al. (2008) 3C 264: Perlman et al. (2010), 3C 270: Worrall et al. (2010), 3C 273: Sambruna et al. (2001b), 3C 296: Hardcastle et al. (2005b), 3C 346: Dulwich et al. (2009), 3C 371: Pesce et al. (2001), 3C 465: Hardcastle et al. (2005a). (Col. 11) Angular size of the soft X-ray emission in arcsec; (Col. 12) Position angle of the more extended direction in the X-ray image; (Col. 13) Morphology of the optical emission line region as Col. 9; (Col. 14) Angular size of the emission line region in arcsec; (Col. 15) Position angle of the more extended direction in the optical line images; (Col. 16) references for the optical line region properties: 1.) Privon et al. (2008), 2.) Tremblay et al. (2009), 3.) McCarthy et al. (1995), 4.) Baum et al. (1988), 5.) Martel et al. (2004), 6.) Edwards et al. (2009), 7.) Sarzi et al. (2006), 8.) Hes et al. (1996), 9.) Prieto & Zhao (1997), 10.) Hippelein et al. (1996), 11.) Morganti et al. (1992), 12.) Husemann et al. (2008); (Col. 17) host galaxy major axis position angle from de Koff et al. (1996), [(a)] Saripalli & Subrahmanyan (2009) , [(b)] Martel et al. (1999) .

parameter[2] Log ξ = 0–4 and the cloud column density from 10^{21} to 10^{23} cm^{-2}. The results are graphically presented in Fig. 4. With the only exception of a thermal model of very low temperature (kT = 0.1 keV) the various models differ from each other by less than ∼20%.

The main uncertainties in the flux measurements are not related to the choice of the model type or model parameters, but from the (generally low) number of counts. Indeed, in 3 sources (3C 180, 3C 379.1, and 3C 452) the emission from the circumnuclear regions does not reach a 3σ significance. At this stage, we discard 3C 321 from any further analysis due to its complex structure, strongly contaminated by a nearby Seyfert galaxy (Evans et al. 2008). Summarizing, this analysis allows us to measure the soft X-ray fluxes from the extra-nuclear regions in 14 3CR sources.

5. In which sources do we observe extended soft X-ray emission?

We find extended soft X-ray emission in 14 out of the 51 sources considered and for 5 of them we have performed both spectral and photometric analysis. By separating them in spectroscopic classes we have 9 extended (and 3 possibly extended) images among the 33 HEGs, with a detection fraction of ∼36%.

In the 18 BLOs, extended emission is seen only in 2 objects; the lower detection rate in BLOs with respect to HEG might be due to the presence of their bright X-ray nuclei, possibly outshining any genuine diffuse emission. We explore this interpretation, by testing whether the typical extended emission in HEGs would have been detected also in BLOs.

The count rates seen in the extended soft X-ray regions of HEGs is in the range $\sim 0.2 \times 10^{-3}$–2×10^{-3} counts/s, with the only exception of 3C 305 where it reaches 2×10^{-2} counts/s. The regions extend from ∼2″ from the nucleus out to a radius of ∼5–10″. We then estimated the count rate produced by the PSF wings of the BLO in the same spatial regions which is typically between $\sim 4 \times 10^{-3}$–6×10^{-3} counts/s. Therefore, an extended X-ray emission with a surface brightness similar to that seen in the HEG would be a factor between 2 and 30 with respect to that associated with the nuclear source. This implies that even in the presence of genuine soft X-ray extended emission in BLOs, similar to that observed in the HEGs, this would not be generally detected from the analysis of the surface brightness profiles nor would induce a significant asymmetry.

We then look for a relation between the soft X-ray extended emission and the radio properties, i.e., the size and the luminosity of the radio source. In Fig. 5 we plot the radio size and luminosity and we highlight the sources that show an extended soft X-ray emission. We find that the fraction of extended objects does not depend on either their size or radio-power. Similarly, no dependence on redshift is seen.

The stronger link is found, rather obviously, with the length of the *Chandra* observations. Indeed, considering only the exposures with $t_{\rm exp} > 10$ ks, we find that 75% (6 out of 8) of the HEGs show extended regions, against 13% (3/23) of the sources observed with $t_{\rm exp} \lesssim 10$ ks. By including the possibly extended and the complex sources, the percentages increase to 80% and 26% for the two classes, respectively.

[2] Defined as $\xi = \frac{L}{nR^2}$ [erg cm s^{-1}], where L is the luminosity of the ionizing source [erg s^{-1}] integrated between 1 and 1000 Rydberg, n is the gas density [cm^{-3}], and r is the distance of the ionizing source from the absorbing gas [cm].

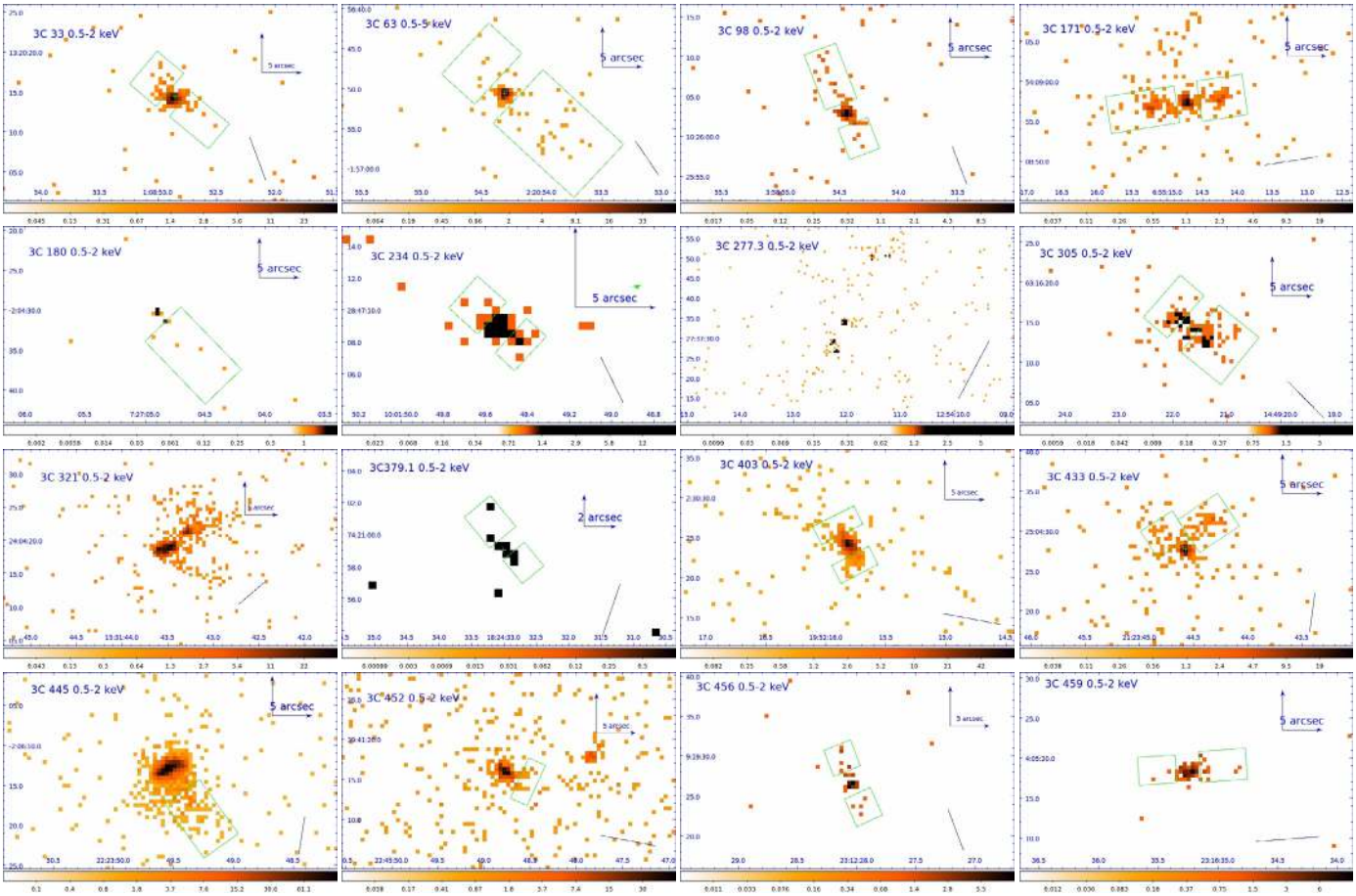

Fig. 1. Images in the soft X-ray band for the 14 sources classified as extended or possibly extended in Table 1 (plus the complex source 3C 321 and the "blobby" source 3C 277.3). The images are unbinned (the pixel size is 0.49″) and we indicate the orientation of the radio axis. When extended emission is present, we superposed the region used for the spectral extraction.

Summarizing, we find that when a 3CR source fulfills two requirements, i.e., the absence of a bright nucleus and when long *Chandra* observations are available, a soft X-ray extended emission is normally observed implying that this is a general characteristic of radio galaxies. As shown in the next section, however, the best predictor of the X-ray properties is represented by the morphology and the strength of the optical emission line region.

6. Comparison between X-ray and optical emission

As discussed in the Introduction, a connection between X-ray, radio, and optical emission lines has been found in several active nuclei, both radio-quiet and radio-loud. We now explore the possibility that this applies in general to a large sample of radio galaxies.

6.1. Optical emission-line images

We search in the literature for optical emission line images for the sources classified in the soft X-rays images as extended or possibly extended, according to Table 1. About 3/4 of them have been imaged with narrow band filter (usually centered on [O III] or Hα+[N II]) with ground based or HST observations. More specifically, we have access to the new re-calibrated HST/ACS images (Tremblay et al. 2009; Rodriguez Zaurin et al., in prep.) (3C 33, 3C 180, 3C 234, 3C 285) and to the HST/WFPC2 images published by Privon et al. (2008) (3C 171, 3C 305, 3C 321, 3C 379.1, 3C 452). In other cases (3C 63, 3C 98, 3C 433, 3C 403, 3C 445) we reproduced and superposed contours from published images (mostly from McCarthy et al. 1995; Baum et al. 1988). Only for 3C 456 we could not find any optical line image.

In order to register the *Chandra* and optical images, we align the centroid of the hard X-ray emission with the peak of the optical emission line structure.

In Fig. 6 we superposed the X-ray contours onto the HST [O III] line images, while in Fig. 7 we present soft X-ray images with superposed ground based optical line contours. In Table 1 we report the main morphological parameters characterizing the sources in the different bands.

6.2. Relationship between X-ray, lines, and radio structures

Overall, we find a very strong correspondence between the morphology of the NLR and the soft X-ray emission. In most cases the two structures are closely co-spatial, an effect particularly clear when we focus on the objects classified as "extended". Despite the difficulties in defining the size of structures measured in images with widely different levels of resolution and sensitivity, we find an excellent match between the NLR and soft X-ray extension.

In Fig. 8 (left panel) we show the histogram of the difference between the direction of the extended emission in optical lines and soft X-ray; this offset can be measured reliably in

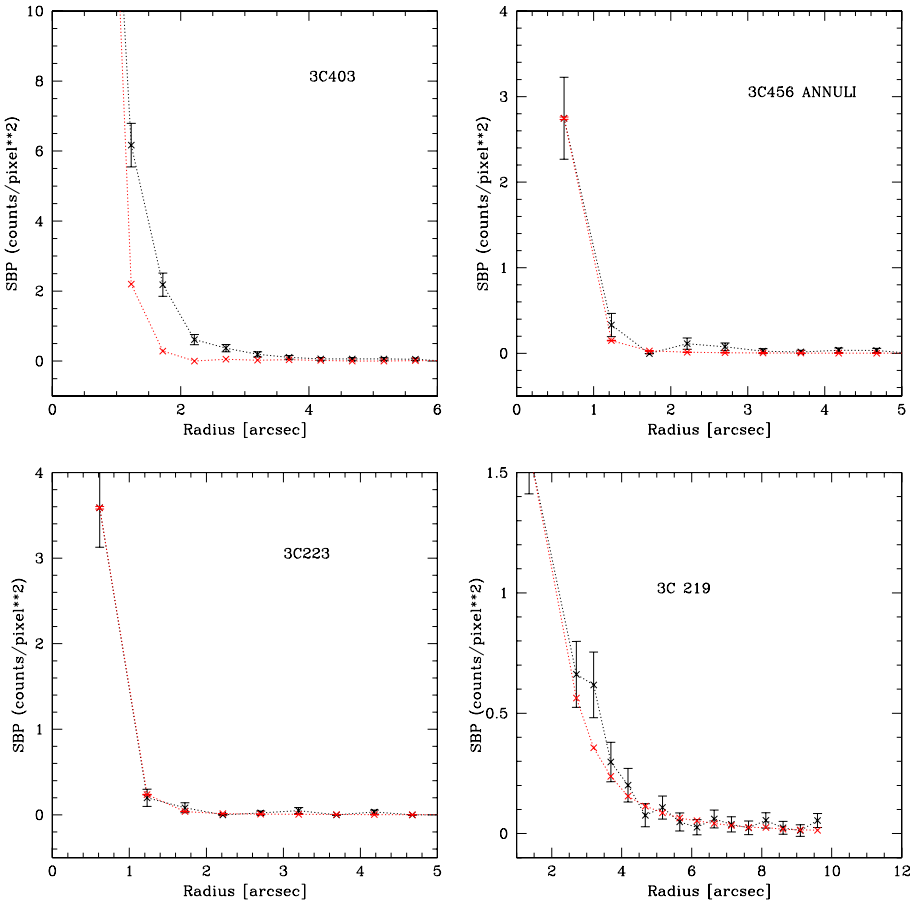

Fig. 2. Comparison of the observed SBP (black) with the PSF profile (red) for 4 representative examples. *Top left*: 3C 403, an "extended" object. Rebinning from 3 to 5 pixels we obtain an excess significant at 9.4σ. *Top right*: 3C 456, an "asymmetric" object. Rebinning from 5 to 9 pixels, we obtain an excess with a significance of 2.5σ, but the difference of the counts considering two orthogonal boxes (one parallel to the radio axis, the second perpendicular to it) centered on the nucleus, is significant at 3.5σ. *Bottom left*: 3C 223, an "unresolved" object. *Bottom right*: the BLO 3C 219. The emission seen at large radii is well reproduced by the wings of the nuclear point source, with only a marginal (1.4σ) excess, and no significant asymmetry is found comparing the two orthogonal boxes. We consider this object to be "unresolved".

12 sources (see Table 1). A very strong alignment is found, with 10/12 sources aligned within 30°.

Only two sources show a high apparent offset between the NLR and the X-ray emission. In 3C 452 the NLR is very compact and its PA measurement is highly uncertain and in 3C 98 the X-rays are produced in a narrow structure, ∼13″ long, well aligned with the Northern radio jet, while the NLR is offset by ∼30°.

In Fig. 8 (middle panel) we show instead the differences between the position angle of the radio emission and of the extended soft X-ray region. Although a clear preference toward small offsets is seen, the distribution is much broader than that of line versus X-ray. In this respect six objects are particularly notable (namely, 3C 33, 3C 379.1, 3C 403, 3C 433, 3C 445 and 3C 452) all showing a very well defined soft X-ray extended region which is misaligned by 30° to 60° from the radio axis, while they are all aligned within a few degrees with the NLR.

Finally, we consider the possibility of a connection between the host galaxy major axis and the soft X-ray emission (see Fig. 8, right panel); such a link can be envisaged as the result of X-ray emission associated with the host hot corona or with star forming regions. The distribution of their differences is essentially flat, arguing against a link between them.

6.3. Notes on individual sources

3C 33: in the soft X-ray band the nuclear structure is clearly extended, with the emission elongated along NE-SW axis. There is a remarkable spatial coincidence with the [O III] emission line region, as already noticed by Kraft et al. (2007) and Torresi et al. (2009).

3C 98: the soft X-ray emission forms a ∼13″ narrow structure well aligned with the Northern radio jet (Leahy et al. 1997).

3C 171: the soft X-ray emission is clearly extended and aligned along the radio axis. This source has been studied in detail by Hardcastle et al. (2010).

3C 180: the biconical structure seen in optical line imaging does not have a clear X-ray counterpart in our short exposure time *Chandra* image. It just reveals a few counts aligned in the same general direction.

3C 234: the emission line region and the soft emission are both aligned with the radio axis.

3C 277.3: two blobs of X-ray emission are seen to the SW of the nucleus. They are cospatial with the two radio knots K1 and K2, associated with regions of line emission (van Breugel et al. 1985) that are also visible in optical and infrared HST images (Capetti et al. 2000; Madrid et al. 2006). The same association between radio, X-ray, and emission line is seen North of the nucleus at the location of the Northern radio hot-spot.

3C 305: the soft X-ray emission extends beyond the radio one and it is cospatial with the optical emission line region (Massaro et al. 2009).

3C 321: this source has a companion galaxy, that also harbors an AGN (Evans et al. 2008). The X-ray emission extends over a large region that includes both galaxies. Due to the complexity of this source, it is not trivial to separate the extended emission associated with each individual active nucleus.

3C 379.1: the soft X-ray and the [O III] emissions are rather compact and cospatial, but not aligned with the radio axis.

3C 445: the *Chandra* image is off-axis (the aim-point was on the Northern hot-spot) and the PSF is elongated along the North-West axis. Instead, the extension of about 10″ along PA

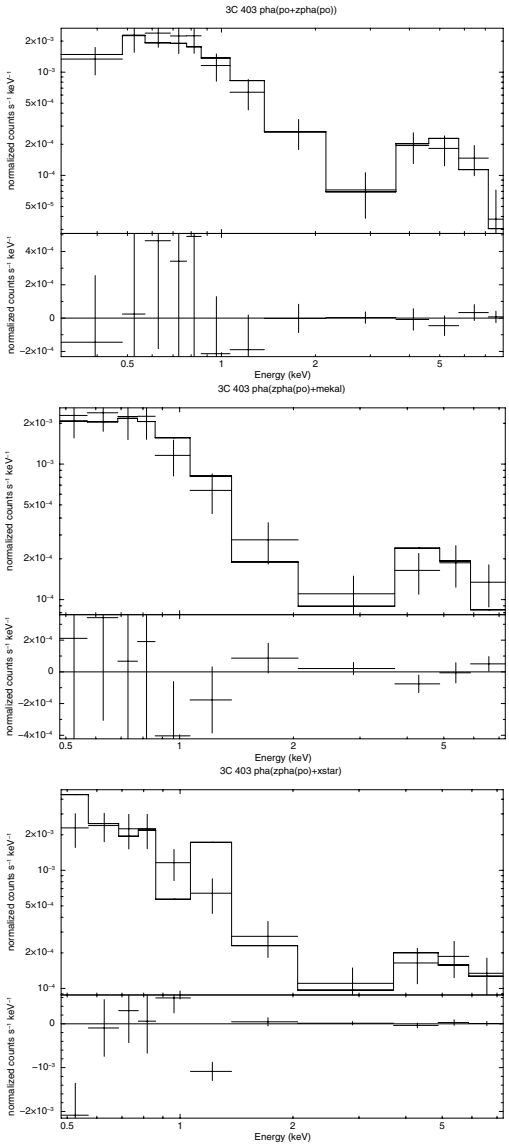

Fig. 3. We report, as an example, the spectrum of 3C 403 in the extended regions fitted with three different models: power-law, MEKAL, and XSTAR, absorbed by a Galactic column density value. We add to the model an intrinsically absorbed power-law to reproduce the emission seen at higher energies (due to the leaking of the nuclear emission).

of ∼135° is real. A similar elongation is visible in the *V* band ground based image published in Heckman et al. (1986). These authors claim that this region is a source of emission lines. This result is confirmed by our TNG spectroscopic observations (see Fig. 9) that were coincidentally obtained with the long-slit aligned with this feature and that shows emission line extending ∼8″ from the nucleus.

6.4. A quantitative comparison of emission lines and soft X-ray structures

In order to quantitatively compare the optical line and the soft X-ray emission, we measure the [O III] flux in the available HST images using the same regions chosen for the X-ray spectral analysis drawn in Fig. 1.

Due to the difficulty to obtain an accurate flux calibration for the HST/WFPC2 ramp filter images (available for 3C 171, 3C 305, 3C 379.1, and 3C 452), we decided to use the information published by Buttiglione et al. (2009) obtained from the ground based TNG spectra. We derive a conversion factor between counts and fluxes by measuring the counts in the HST images in the same 2″ × 2″ nuclear extraction region used by Buttiglione et al. (2009) to measure the line fluxes (accurate to ∼10%). The resolution of the HST images has been previously degraded, with a Gaussian smoothing, to match the resolution of each TNG observation. This scaling factor has been applied to the counts measured in the extra-nuclear regions to estimate line fluxes.

Two of the sources of our sample (namely, 3C 445 and 3C 403) were not observed with HST with the ramp filters. However, these objects were observed by Buttiglione et al. (2009). In those observations the long slit was, by chance, oriented in the same direction as the PA of the X-ray extended emission. For these sources we extracted the X-ray spectrum in the same region covered by the 2″ wide slit (see Fig. 9).

We corrected all line fluxes for reddening due to the Galaxy using the extinction law of Cardelli et al. (1989) and the galactic $E(B-V)$ value for each object as tabulated by Buttiglione et al. (2009), taken from the NASA Extragalactic Database (NED).

In Table 3 we report the resulting [O III] and soft X-ray fluxes, the corresponding luminosities, and their ratio, $\mathcal{R}$([O III]/sX). The median ratio of $\mathcal{R}$([O III]/sX) is 5.6 and the scatter is low, with all sources confined to within a factor ∼2 from the median value. No dependence of $\mathcal{R}$([O III]/sX) on luminosity is found. The line and X-ray fluxes are graphically compared in Fig. 10.

For this same group of 9 sources, we estimated $\mathcal{R}$([O III]/sX) also on the nucleus. We find values even more closely clustered, all falling within a factor of ∼1.3 from the median value of 2.4, a factor of ∼2 lower than in the extended regions.

7. Discussion

7.1. Origin of the soft X-ray emission

The presence of extended soft X-ray emission can be attributed to various mechanisms:

- thermal emission from hot gas, collisionally ionized and/or compressed by a jet or an outflow;
- nuclear X-ray emission scattered by an extended medium;
- non thermal emission from i) synchrotron (or inverse Compton) radiation from the radio-jets and hot-spots; or ii) inverse Compton scattering of low energy photons by the relativistic electrons in the radio lobes;
- emission from gas photoionized by the nuclear source.

In order to identify the emission process responsible for the X-ray emission, the most powerful tool is clearly a direct spectral fit. The model that better reproduces the observed spectrum not only identifies the radiation mechanism but also constraints the physical parameters of the emitting medium. With respect to previous studies based on individual sources we can now look for a common process that accounts for the X-ray spectra observed for this whole group of galaxies. For the 3CR sources considered here, in 5 cases it is possible to follow this approach (see Sect. 4 and Table 2).

Nonetheless, the results presented in Sect. 4 are not sufficient to securely identify the emission mechanism at work in these sources, mainly due to the low number of counts. There is not a unique model that proves to be superior in fitting every source, or, on the contrary, that does not provide a reasonable agreement

Table 2. Results of the spectral fits for the extended emission of the 5 sources with the highest number of counts.

Name	Model name	Model parameters	Nuclear component	χ^2_ν (d.o.f.)	F(0.5–2 keV)
3C 171	pha(mekal+zpha(po))	$kT = 1.3^{+0.3}_{-0.2}$ [keV] $ab = 0.03^{+0.1}_{-0.02}$	Γ = 1.7fix zNh = 8.8e22 [cm^{-2}] fix	1.25(4)	1.19e–14
		ab = 0.3 fix		1.83(5)	
		ab = 0.5 fix		2.26(5)	
	pha(pow+zpha(po))	$\Gamma = 3.1^{+0.5}_{-0.5}$	Γ = 1.7fix zNh = 8.8e22 [cm^{-2}] fix	1.26(5)	1.33e-14
		Γ = 1.7 fix		4.76(6)	
	pha(xstar+zpha(po))	$N = 2.2^{+0.3}_{-2.2}$e21 [cm^{-2}] $\log\xi = 2.5^{+0.6}_{-0.1}$	Γ = 1.7fix zNh = 8.8e22 [cm^{-2}] fix	0.94(4)	1.89e-14
3C 305	pha(mekal)	$kT = 1.06 \pm 0.1$ [keV] ab = 0.3 fix			4.17e-14
	pha(po)	$\Gamma = 2.5 \pm 0.2$			4.62e-14
	pha(xstar)	$N = (2.17 \pm 0.09)$e21 [cm^{-2}] $\log\xi = 5.0 \pm 1.0$			4.07e-14
3C 403	pha(mekal+zpha(po))	$kT = 0.38 \pm 0.05$ [keV] $ab = 0.00 \pm 0.01$	Γ = 1.7fix zNh = (19.7 ± 5.2) e22 [cm^{-2}]		9.12e-15
	pha(pow+zpha(po))	$\Gamma = 3.9 \pm 0.3$	Γ = 1.7fix zNh = (24.1 ± 7.1) e22 [cm^{-2}]		8.97e-15
	pha(xstar+zpha(po))	$N = (8.3 \pm 12.0)$e23 [cm^{-2}] $\log\xi = 5.0 \pm 3.3$	Γ = 1.7fix zN = (18.8 ± 6.8)e22 [cm^{-2}]		1.25e-14
3C 433	pha(mekal+zpha(po))	$kT = 0.7 \pm 0.1$ [keV] $ab = 0.1 \pm 0.09$	Γ = 1.7fix zNh = (8.6 ± 2.1)e22 [cm^{-2}]		1.04e-14
	pha(pow+zpha(po))	$\Gamma = 3.5 \pm 0.5$	Γ = 1.7fix zNh = (10.3 ± 2.8)e22 [cm^{-2}]		1.03e-14
	pha(xstar+zpha(po))	$N = (9.9 \pm 2.7)$e21 [cm^{-2}] Log $\xi = 3.9 \pm 1.2$	Γ = 1.7fix zNh = (12.1 ± 3.4)e22 [cm^{-2}]		1.15e-14
3C 445	pha(mekal+zpha(po))	$kT = 0.39 \pm 0.05$ [keV] $ab = 0.00 \pm 0.01$	Γ = 1.7fix zNh = (11.0 ± 6.5)e22 [cm^{-2}]	0.85(4)	1.46e-14
		ab = 0.3 fix		2.84(5)	
		ab = 0.5 fix		2.91(5)	
	pha(pow+zpha(po))	$\Gamma = 3.7 \pm 0.2$	Γ = 1.7 fix zNh = (14.7 ± 7.9)e22 [cm^{-2}]	1.22(5)	1.03e-14
		Γ = 1.7 fix		10.89(6)	
	pha(xstar+zpha(po))	$N = (1.1 \pm 0.1)$e22 [cm^{-2}] Log$\xi = 5.0 \pm 3.4$	Γ = 1.7fix zNh = (15.9± 8.6)e22 [cm^{-2}]	2.45(4)	1.59e-14

Notes. For 3C 305, 3C 403, and 3C 433 the spectrum is grouped to at least 10 counts/bin and we apply a Poissonian statistic (cstat). The fluxes reported in the table are corrected for Galactic absorption. For 3C 171 and 3C 445 the spectrum is grouped by at least 20 counts/bin (χ^2 statistic). In four cases we add in the models a power-law component to fit the emission observed in the hard band. Notes. 3C 171: in all the models, we fixed the nuclear component parameters at $\Gamma = 1.7$ and $N_H = 8.8 \times 10^{22}$ cm^{-2} (see Hardcastle et al. 2010); 3C 305: the spectrum do not require a nuclear related component. We do not report in table the flux measurement if the model is not representative of the spectrum (according to the χ^2 value).

Table 3. Results for the 14 sources for which it was possible to carry out a spectral analysis.

Name	N_H 10^{20} [cm^{-2}]	cts	S/N	F(0.5–2 keV) [10^{-14} erg cm^2 s^{-1}] pha(po)	pha(mek)	pha(xstar)	L(0.5–2 keV) 10^{41} [erg s^{-1}]	$F_{[O\ III]}$ 10^{-14} [erg cm^2 s^{-1}]	$L_{[O\ III]}$ 10^{41} [erg s^{-1}]	$F_{[O\ III]}/F_{sX}$ ext	$F_{[O\ III]}/F_{sX}$ nuc
3C 33	3.23	44	6.5	0.904	0.829	1.78	1.48	5.92	4.91	3.3	2.3
3C 63	2.47	31	5.4	1.77	1.72	1.89	15.8				
3C 98	10.2	25	4.7	0.592	0.587	0.805	0.171				
3C 171*	5.65	134	11.3	1.15	1.52	1.34	30.4	3.09	51.8	2.3	3.1
3C 180	13.6	6	2.3	<0.664	<0.736	<0.846	<11.8	1.80	698	>2.1	
3C 234	1.76	13	3.6	0.670	0.651	0.715	6.75	4.13	39.1	5.8	2.5
3C 305*	1.31	89	9.3	4.38	3.98	4.87	1.92	11.1	4.36	2.3	2.3
3C 379.1	5.43	3	1.7	<0.266	<0.280	<0.317	<6.24	0.332	6.54	>1.04	
3C 403*	12.2	51	7.0	0.494	0.467	0.641	0.520	4.79	3.89	7.5	2.0
3C 433*	7.77	83	8.7	1.01	0.971	1.27	3.25				
3C 445*	4.49	92	9.2	0.884	0.816	1.03	0.756	3.60	2.64	3.5	3.8
3C 452	9.64	12	2.3	<0.06	<0.0594	<0.0736	<0.117	0.467	0.738	>6.3	1.5
3C 456	3.70	11	3.2	0.597	0.606	0.670	14.4				
3C 459	5.24	13	3.6	0.739	0.754e	0.858	11.9				

Notes. We mark with a star symbol the 5 sources with a sufficiently high number of counts for which we perform in addition a spectral fit. We converted the observed number counts in a flux value adopting three different models: a power-law, mekal, or Xstar, absorbed by the Galactic N_H column density. We report the unabsorbed soft X-ray fluxes for all 3 models and the luminosity for the XSTAR model in the soft X-ray band (0.5–2 keV). We also give the [O III] flux and luminosity in the same regions used for the extraction of the X-ray spectra.

with the data in all of them. However, some general trends can be seen.

We find that power-law models require rather high values of the spectral index, $2.5 < \Gamma < 3.9$, while extremely low values of the abundance are highly favored for the thermal models and the best fit are often obtained with an effectively null metallicity. Our results are fully consistent with the analysis of 3C 171 by Hardcastle et al. (2010) and of Bianchi et al. (2006) in their analysis of the extended X-ray emission from Seyfert 2 galaxies.

These findings cast doubts on the physical sensibleness of these models. Indeed in case of a power-law emission resulting from scattering of nuclear light from gas located in the extended regions, the spectral index is expected to be preserved and to be equal to that observed in the nucleus. The measured values

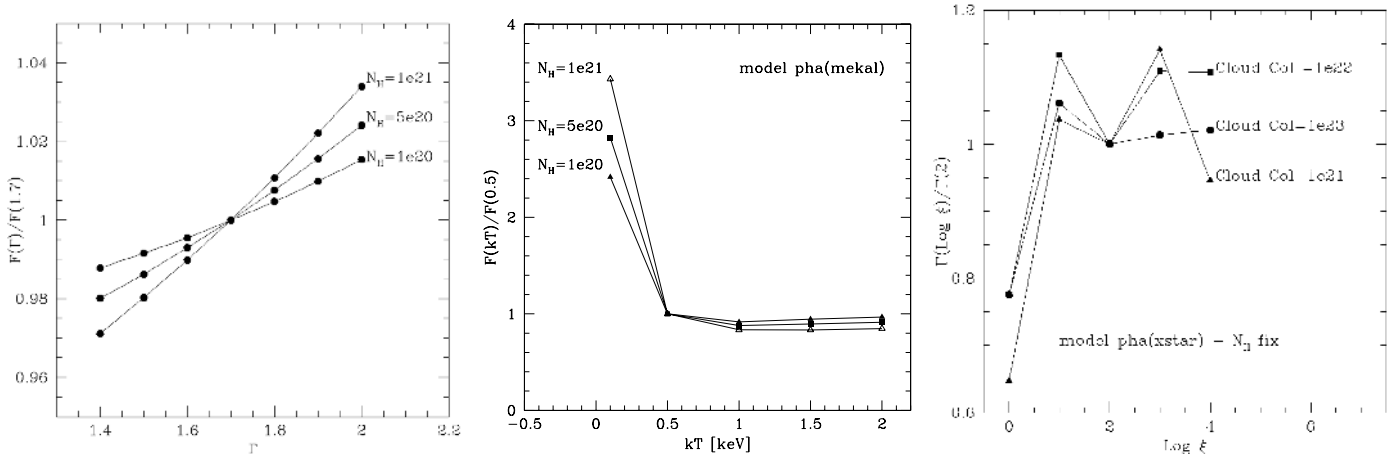

Fig. 4. For the three different models considered, phabs (pow), phabs (MEKAL), and phabs (XSTAR), we evaluate the flux variations in the 0.5–2 keV range due to changes in the most important parameters of the models (see Sect. 4). These values have been calculated for a source at the aim-point in ACIS/S.

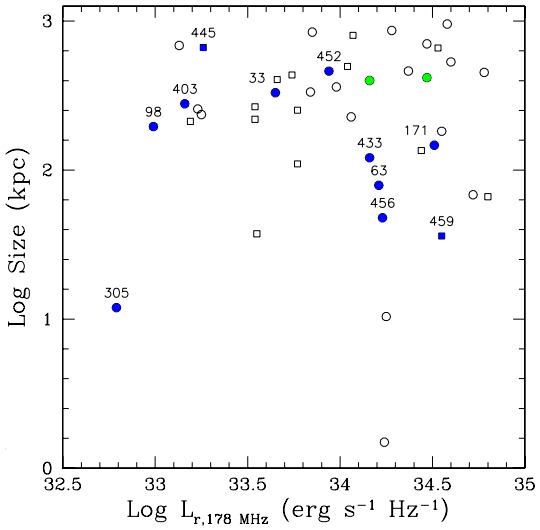

Fig. 5. Radio luminosity vs. radio size for the 3CR HEG and BLO sources. Circles are HEGs, squares are BLOs. We marked with a solid blue sign the sources with extended soft X-ray emission (for which we also show the galaxy's name) and with green symbols the partially extended sources.

of Γ in our sources are instead much larger than those usually observed in both radio-quiet and radio-loud AGN (e.g. Bianchi et al. 2009). High energy emission from the radio jets or hot spots can already be generally excluded on a morphological basis (since it requires a close cospatiality of X-ray and radio emission, not observed in these 5 sources) but also on the typical spectral index measured from objects in which this is clearly the dominant emission process (Harris & Krawczynski 2006). Similarly, the location of the soft X-ray emission in our sources is concentrated within a few kpc from the nucleus and it does not originate from the large scale radio lobes as expected in the case of IC emission described above. Concerning the value of metallicity derived from the spectral fits, note that the metallicity of the interstellar medium in early-type galaxies is only slightly sub-solar (Fabbiano 1989; Humphrey & Buote 2006). Furthermore, the optical NLR that, as shown in Sect. 6.2, is cospatial with the soft X-ray emission, usually have super solar metallicities (Storchi-Bergmann et al. 1996).

In order to assess whether these models can still provide a good fit to the data with more realistic parameters, we forced them to be in a physically acceptable range, fixing (for the thermal model) $\mu = 0.5$ solar and (for the power-law models) $\Gamma = 1.7$. For the two sources where we have a sufficient number of counts to use a χ^2 statistics we find that quality of the fits worsens significantly (see Table 2).

When considering the XSTAR model, it generally provides a reasonably good fit to the data of all five sources. In 3C 171 XSTAR corresponds to the smaller χ^2 value, and the better quality with respect to those obtained with MEKAL and power-laws is strongly increased when we limit to models with values fixed to acceptable values, as explained above. In 3C 445 the preference for XSTAR emerges only against the latter set of models. Unfortunately the parameter values obtained with the XSTAR have large errors and thus we obtain only very limited information on the physical condition of the emitting gas. This is the same general result obtained from similar studies that can be found in the literature (e.g. Ogle et al. 2003).

Nonetheless, in the light of the results of the somewhat limited spectral modeling possible with the available data, the favored mechanism to account for the extended soft X-ray regions appears to be emission from a photoionized plasma.

Although no spectral analysis was possible for those sources with low count rates, the soft X-ray fluxes in their extended regions can still generally be estimated (as discussed in Sect. 6.2). The comparison of the soft X-ray and [O III] line fluxes, possible for 11 galaxies, shows a strong connection between the emission in the two bands, with all sources confined to within a factor ~2 from the median value of 5.6. Interestingly, this same result is found considering their nuclear regions, see Table 2, with an only slightly decreased median ratio of 2.4. Furthermore, the $\mathcal{R}$([O III]/sX) ratios in the 3CR sources are in remarkable coincidence with those measured in the Seyfert 2 galaxies by Bianchi et al. (2006) that cover the range $\mathcal{R}$([O III]/sX) = 2.8−4.8 (with only one object with $\mathcal{R}$([O III]/sX) = 11). The small range in the ratios between optical lines and soft X-ray emission and the similarity with those measured in their nuclear regions points to a common mechanism for the emission in these two bands over both the nuclear and the extended regions.

As already mentioned in the Introduction, the few X-ray spectroscopic studies for the nuclear regions of radio galaxies show that the dominant radiation mechanism is associated with

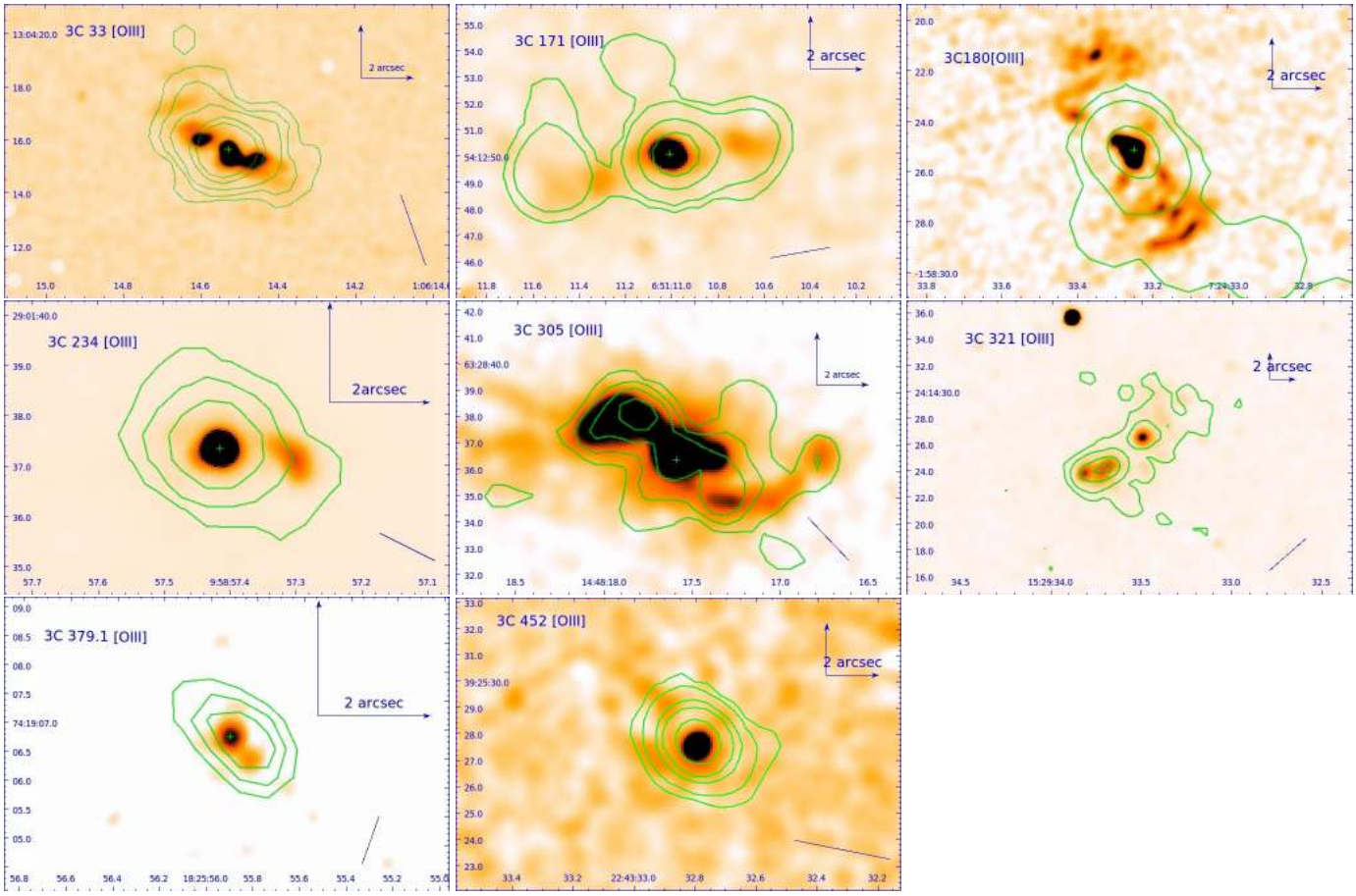

Fig. 6. Green iso-counts contours of the soft X-ray emission (0.5–2 keV), superposed onto the HST [O III] images (smoothed with 0.″3 Gaussian kernel). Contours for the various sources are drawn at the following levels of counts pixel^{-1}: 3C 33 (0.2, 0.5, 1, 3, 5, 20), 3C 171 (0.05, 0.1, 0.3, 0.5), 3C 180 (0.01, 0.05, 0.2), 3C 234 (0.2, 1, 4), 3C 305 (0.2, 0.5, 1, 2), 3C 321 (0.4,2, 10, 20), 3C 379.1 (0.1, 0.2, 0.3), 3C 452 (0.5, 1, 3, 5, 10).

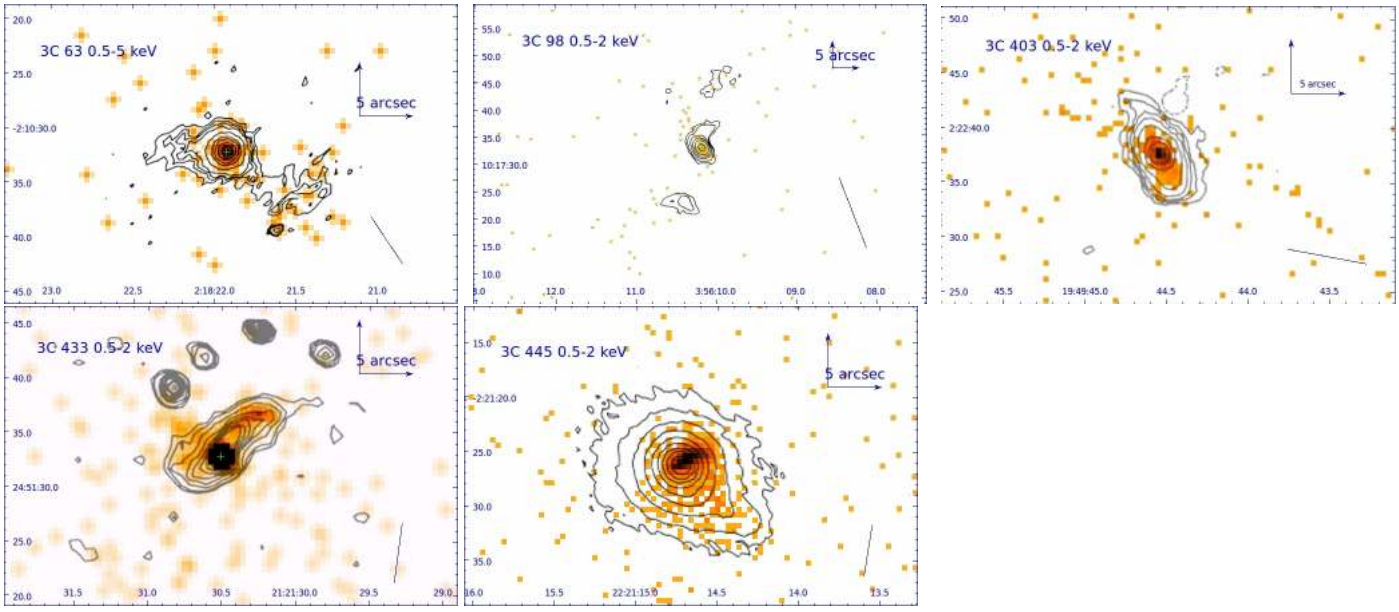

Fig. 7. Comparison between soft X-ray emission (0.5–2 keV) and narrow line region (mapped usually by [O III] or Hα+[N II]). We reproduced and superposed optical line contours from published images on the *Chandra* images. 3C 63, 3C 403, 3C 433: Hα+[N II] contours from Baum et al. (1988). 3C 98: Superposed [O III] contours are from Hansen et al. (1987). 3C 445: the *Chandra* image is off-axis causing a PSF elongation along the north-west axis. Instead the extension of about 10 arcsec along PA ~135° is real and also visible in the *V* band ground based observation published in Heckman et al. (1986) (contour superposed).

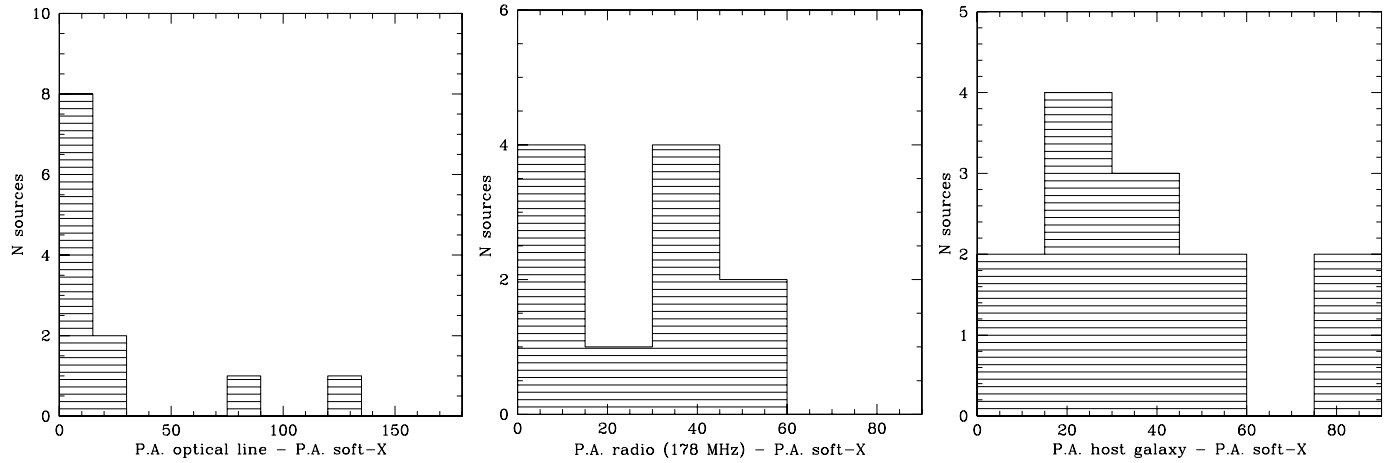

Fig. 8. Histograms of the offset between the position angle (PA) of extended regions measured in soft X-ray, with respect to the narrow line region (*left*), the radio emission (*middle*), and the host galaxy's major axis (*right*).

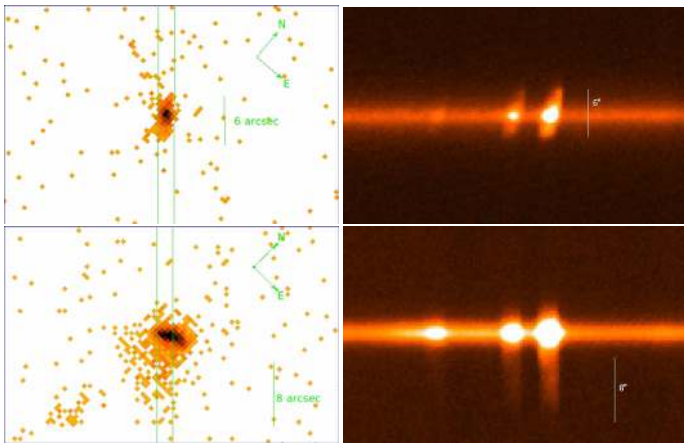

Fig. 9. *Left panels*: rotated *Chandra* soft X-ray images for 3C 403 (*top*) and 3C 445 (*bottom*) with the superposed 2″ wide slit used to obtain the spectra at the TNG shown in the *right panels*. The three emission lines are Hβ and the [0 III]$\lambda\lambda$4959, 5007 doublet. Substantial line emission is produced along the direction of the soft X-ray emission. The sizes of the two emitting regions (in line and X-rays) are similar.

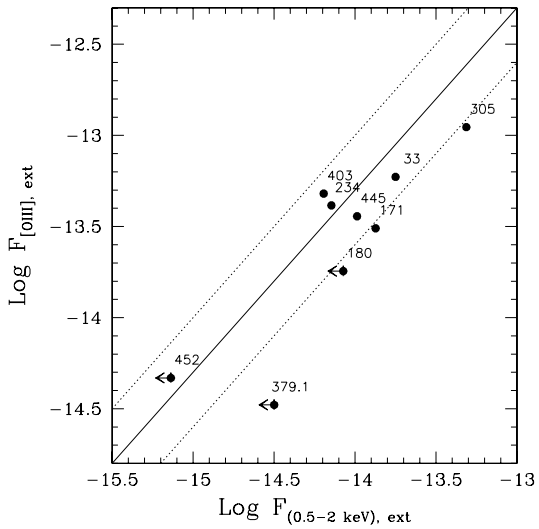

Fig. 10. Comparison of the [O III] and soft X-ray fluxes measured in the extended regions drawn in Fig. 1. The solid line corresponds to a constant ratio F([O III])/F(soft X-ray) = 5; the two dashed lines mark a ratio equal to 2.5 and 10.

the presence of photoionized gas. This same result is obtained from the studies of both the nuclear and extended regions in Seyfert galaxies. This indicates that, in presence of photoionized gas, a strong link between soft X-ray and optical emission lines fluxes arises naturally. This argues in favor of an interpretation in which the extended X-rays seen in the 3CR sources are also due to a collection of emission lines.

A further element in favor of a line origin for the soft X-ray emission is the close spatial connection with the optical lines. We found only one clear exception (3C 98) and a second complex case (3C 277.3) that we discussed in Sect. 6.3. In all other sources the available optical line images show a remarkable spatial coincidence with the morphology of the extended X-ray emission. Again, in Seyfert galaxies there is similar close spatial association between [O III] and X-ray morphology.

8. Summary and conclusions

We analyzed the diffuse soft X-ray emission (0.5–2 keV) of the 3CR radio galaxies at $z < 0.3$. Extended soft X-ray emission has been observed in Seyfert galaxies and also in a few radio galaxies, usually matching very well the morphology of the optical emission line region. In order to characterize and constrain the physical mechanism that produce the observed soft X-ray emission, we take advantage of this large and complete sample, now entirely observed by *Chandra*. We here focused on the properties of the spectroscopic sub-classes of high excitation galaxies and broad line objects.

We performed an imaging analysis, describing the morphology of the extended features and measuring their sizes and position angles. In the 33 HEGs we detected extended (or possibly extended) emission in about 40% of the sources; the fraction is even higher (8/10) restricting the analysis to the objects with exposure times larger than 10 ks.

In the 18 BLOs, extended emission is seen only in 2 objects; this lower detection rate can be ascribed to the presence of their bright X-ray nuclei that easily outshine any genuine diffuse emission.

The count rates seen in the extended soft X-ray regions of HEGs is in the range $\sim 0.2 \times 10^{-3}$–2×10^{-3} counts/s, with the only exception of 3C 305 where it reaches 2×10^{-2} counts/s.

The regions extend from ∼2″ from the nucleus out to a radius of usually ∼5−10″. We estimated that the count rate produced by the PSF wings of the BLO in the same spatial regions is typically between $\sim 4 \times 10^{-3}$–6×10^{-3} counts/s. Therefore, an extended X-ray emission with a surface brightness similar to that seen in the HEG would be a factor between 2 and 30 with respect to that associated with the nuclear source. This implies that even in the presence of genuine soft X-ray extended emission in BLOs, similar to that observed in the HEGs, this would not be generally detected from the analysis of the surface brightness profiles nor would induce a significant asymmetry.

Thus, a soft X-ray extended emission is a general characteristic of radio galaxies. With respect to previous studies based on individual sources, we can here look for a common mechanism that can reproduce the properties of these galaxies, revealing a common process that accounts for the X-ray spectra observed.

We consider different scenarios: scattered nuclear light, emission from collisionally ionized plasma, non-thermal radiation, and emission from photoionized gas. Among these various possibilities we argue that the most plausible dominant process is AGN photoionization based on the following results:

- The first clue is the impressive morphological similarity between the optical NLR and the soft X-ray emission regions. The offsets between soft X-ray and optical lines axis are generally very small, $\lesssim 20°$. Instead the offsets distribution between soft X-ray, radio and optical galaxy axis are much broader.
- The fluxes of the [O III] optical line and of the soft X-ray emission in the extended regions are strongly correlated (with a scatter of less than a factor of 2), suggesting that they are produced by the same mechanism. Furthermore, the ratio of [O III]/soft X-ray fluxes is very similar to that observed in the nuclear regions of radio galaxies and in both the extended and nuclear regions of Seyfert galaxies. For these latter sources the origin of the soft X-ray emission from photoionized gas is well established.
- In 5 sources the counts in the soft band are sufficient to perform a spectral analysis. Although we are not able to securely identify the emission mechanism at work in these sources, a photoionized gas model (XSTAR in XSPEC) always provides an acceptable fit to the data. Unfortunately the resulting parameters values have large errors and provides us with only very limited information on the physical condition of the emitting gas. Nonetheless, the resulting values for the ionization parameter obtained in this framework are in the range $\log \xi \sim 2.5$–5, consistent with the median value of ~ 4.8 erg s^{-1} cm found by Tombesi et al. (2010), exploring the properties of ultra fast outflows in a sample of broad-line radio galaxies. Given the large change in radius going from pc to kpc scale, this requires a strong decrease in the gas density to maintain an approximately constant ionization parameter, that can be obtained with a gas density decreasing roughly proportionally to r^{-2}. This is in line with the limited information of spatially resolved changes of ξ with radius (e.g. Bianchi et al. 2006). In this scenario, the soft X-rays radiation arises from emission lines originating from tenuous, hot gas cospatial with the clouds producing the optical lines.

The weaknesses of the alternative scenarios are mainly due to the results of the limited spectral fitting we can perform with the available data. Indeed, in case of scattered nuclear radiation from free electrons we expect the spectral index of the incident power-law to be preserved; instead we obtained values much larger than those usually observed in AGN. Similarly, emission from hot gas reproduces the 5 available spectra only adopting an effectively null metallicity. However, the main strength of the photoionized gas scenario is that it naturally reproduces the close correspondence between optical lines and soft X-ray emission, both in terms of morphology and of relative intensity, being due to a common mechanism. In case of scattering or of emission from hot gas, a certain level of co-spatiality can be expected (see e.g. the correspondence between polarized/scattered light and optical lines in Seyfert galaxies, Capetti et al. 1995, 1996; Kishimoto et al. 2002) but the constant flux ratio with the optical lines appears to be rather contrived.

Finally, we remind that in one source (3C 98) the soft X-ray emission forms a narrow structure well aligned with the jet, in a region devoid of any line emission, a clear evidence that we are observing the high energy counter-part of its radio emission; in another galaxy (3C 277.3) there are two blobs of X-ray emission cospatial with two radio knots, which are however also associated with regions of line emission. These two sources warn us that our approach based on the assumption of a common emission mechanism in all radio galaxies might be oversimplified. For example, we note that the sources with a radio size smaller than ∼100 kpc have a slightly lower [O III]/soft X-ray ratio ($\mathcal{R}$([O III]/sX) < 2.3), suggesting that the gas is in a higher state of ionization, with respect to the bigger sources ($\mathcal{R}$([O III]/sX) > 3). This suggests a possible role of the shocks produced by the interaction of the gas with the jets, particularly important in the smaller radio sources, in which the jet is still expanding through the denser regions of the interstellar medium (Best et al. 2000). This strong interaction is witnessed also by the close alignment of radio, optical, and X-ray emission, and on their disturbed kinematics (Baum et al. 1992).

Acknowledgements. We wish to honor the memory of our great friend and colleague David Axon, who has been the steadfast inspiration and participant in this and many other key papers that through many years of dedicated efforts have led to significant breakthroughs and greater understanding of the physics of active galaxies. He will be greatly missed by all of us. We are grateful to the anonymous referee for usuful comments that significantly improved the paper. We thank also S. Bianchi and G. Matt for helpful comments on the manuscript. This work was mainly supported by the Italian Space Agency through contract ASI-INAF I/009/10/0 and ASI/GLAST I/017/07/0.

References

Antonucci, R. 1993, ARA&A, 31, 473
Baum, S. A., Heckman, T. M., Bridle, A., van Breugel, W. J. M., & Miley, G. K. 1988, ApJS, 68, 643
Baum, S. A., Heckman, T. M., & van Breugel, W. 1992, ApJ, 389, 208
Bautista, M. A., & Kallman, T. R. 2001, ApJS, 134, 139
Best, P. N., Röttgering, H. J. A., & Longair, M. S. 2000, MNRAS, 311, 23
Bianchi, S., Guainazzi, M., & Chiaberge, M. 2006, A&A, 448, 499
Bianchi, S., Guainazzi, M., Matt, G., Fonseca Bonilla, N., & Ponti, G. 2009, A&A, 495, 421
Buttiglione, S., Capetti, A., Celotti, A., et al. 2009, A&A, 495, 1033
Buttiglione, S., Capetti, A., Celotti, A., et al. 2010, A&A, 509, A6
Buttiglione, S., Capetti, A., Celotti, A., et al. 2011, A&A, 525, A28
Capetti, A., Macchetto, F., Axon, D. J., Sparks, W. B., & Boksenberg, A. 1995, ApJ, 452, L87
Capetti, A., Axon, D. J., Macchetto, F., Sparks, W. B., & Boksenberg, A. 1996, ApJ, 466, 169
Capetti, A., de Ruiter, H. R., Fanti, R., et al. 2000, A&A, 362, 871
Cardelli, J. A., Clayton, G. C., & Mathis, J. S. 1989, ApJ, 345, 245
Carilli, C. L., Harris, D. E., Pentericci, L., et al. 2002, ApJ, 567, 781
Crenshaw, D. M., Kraemer, S. B., Hutchings, J. B., et al. 2000, AJ, 120, 1731
Dadina, M., Guainazzi, M., Cappi, M., et al. 2010, A&A, 516, A9
de Koff, S., Baum, S. A., Sparks, W. B., et al. 1996, ApJS, 107, 621
Dulwich, F., Worrall, D. M., Birkinshaw, M., Padgett, C. A., & Perlman, E. S. 2009, MNRAS, 398, 1207
Edwards, L. O. V., Robert, C., Mollá, M., & McGee, S. L. 2009, MNRAS, 396, 1953
Elvis, M., Briel, U. G., & Henry, J. P. 1983, ApJ, 268, 105
Elvis, M., Fassnacht, C., Wilson, A. S., & Briel, U. 1990, ApJ, 361, 459

Evans, D. A., Lee, J. C., Kamenetska, M., et al. 2006, ApJ, 653, 1121
Evans, D. A., Fong, W.-F., Hardcastle, M. J., et al. 2008, ApJ, 675, 1057
Fabbiano, G. 1989, ARA&A, 27, 87
Fanaroff, B. L., & Riley, J. M. 1974, MNRAS, 167, 31
Grandi, P., Guainazzi, M., Cappi, M., & Ponti, G. 2007, MNRAS, 381, L21
Guainazzi, M., & Bianchi, S. 2007, MNRAS, 374, 1290
Hansen, L., Jorgensen, H. E., & Norgaard-Nielsen, H. U. 1987, A&AS, 71, 465
Hardcastle, M. J., Birkinshaw, M., & Worrall, D. M. 2001, MNRAS, 326, 1499
Hardcastle, M. J., Worrall, D. M., Birkinshaw, M., Laing, R. A., & Bridle, A. H. 2002, MNRAS, 334, 182
Hardcastle, M. J., Sakelliou, I., & Worrall, D. M. 2005a, MNRAS, 359, 1007
Hardcastle, M. J., Sakelliou, I., & Worrall, D. M. 2005b, MNRAS, 358, 843
Hardcastle, M. J., Massaro, F., & Harris, D. E. 2010, MNRAS, 401, 2697
Hardcastle, M. J., Massaro, F., Harris, D. E., et al. 2012, MNRAS, 424, 1774
Harris, D. E., & Krawczynski, H. 2006, ARA&A, 44, 463
Heckman, T. M., Smith, E. P., Baum, S. A., et al. 1986, ApJ, 311, 526
Hes, R., Barthel, P. D., & Fosbury, R. A. E. 1996, A&A, 313, 423
Hippelein, H., Meisenheimer, K., & Roeser, H. J. 1996, A&A, 316, 29
Humphrey, P. J., & Buote, D. A. 2006, ApJ, 639, 136
Husemann, B., Wisotzki, L., Sánchez, S. F., & Jahnke, K. 2008, A&A, 488, 145
Kataoka, J., Leahy, J. P., Edwards, P. G., et al. 2003, A&A, 410, 833
Kinkhabwala, A., Sako, M., Behar, E., et al. 2002, ApJ, 575, 732
Kishimoto, M., Kay, L. E., Antonucci, R., et al. 2002, ApJ, 565, 155
Kraft, R. P., Birkinshaw, M., Hardcastle, M. J., et al. 2007, ApJ, 659, 1008
Krolik, J. H., & Vrtilek, J. M. 1984, ApJ, 279, 521
Leahy, J. P., Black, A. R. S., Dennett-Thorpe, J., et al. 1997, MNRAS, 291, 20
Madrid, J. P., Chiaberge, M., Floyd, D., et al. 2006, ApJS, 164, 307
Martel, A. R., Baum, S. A., Sparks, W. B., et al. 1999, ApJS, 122, 81
Martel, A. R., Ford, H. C., Bradley, L. D., et al. 2004, AJ, 128, 2758
Massaro, F., Harris, D. E., Chiaberge, M., et al. 2008, in The X-ray Universe 2008
Massaro, F., Chiaberge, M., Grandi, P., et al. 2009, ApJ, 692, L123
McCarthy, P. J., Spinrad, H., & van Breugel, W. 1995, ApJS, 99, 27
Morganti, R., Ulrich, M.-H., & Tadhunter, C. N. 1992, MNRAS, 254, 546
Ogle, P. M., Brookings, T., Canizares, C. R., Lee, J. C., & Marshall, H. L. 2003, A&A, 402, 849
Perlman, E. S., Padgett, C. A., Georganopoulos, M., et al. 2010, ApJ, 708, 171
Pesce, J. E., Sambruna, R. M., Tavecchio, F., et al. 2001, ApJ, 556, L79
Piconcelli, E., Bianchi, S., Miniutti, G., et al. 2008, A&A, 480, 671
Prieto, M. A., & Zhao, H. 1997, MNRAS, 290, 34
Privon, G. C., O'Dea, C. P., Baum, S. A., et al. 2008, ApJS, 175, 423
Sako, M., Kahn, S. M., Paerels, F., & Liedahl, D. A. 2000, ApJ, 543, L115
Sambruna, R. M., Netzer, H., Kaspi, S., et al. 2001a, ApJ, 546, L13
Sambruna, R. M., Urry, C. M., Tavecchio, F., et al. 2001b, ApJ, 549, L161
Sambruna, R. M., Reeves, J. N., & Braito, V. 2007, ApJ, 665, 1030
Saripalli, L., & Subrahmanyan, R. 2009, ApJ, 695, 156
Sarzi, M., Falcón-Barroso, J., Davies, R. L., et al. 2006, MNRAS, 366, 1151
Spergel, D. N., Verde, L., Peiris, H. V., et al. 2003, ApJS, 148, 175
Spinrad, H., Marr, J., Aguilar, L., & Djorgovski, S. 1985, PASP, 97, 932
Storchi-Bergmann, T., Rodriguez-Ardila, A., Schmitt, H. R., Wilson, A. S., & Baldwin, J. A. 1996, ApJ, 472, 83
Tombesi, F., Sambruna, R. M., Reeves, J. N., et al. 2010, ApJ, 719, 700
Torresi, E., Grandi, P., Guainazzi, M., et al. 2009, A&A, 498, 61
Tremblay, G. R., Chiaberge, M., Sparks, W. B., et al. 2009, ApJS, 183, 278
van Breugel, W., Miley, G., Heckman, T., Butcher, H., & Bridle, A. 1985, ApJ, 290, 496
Wang, J., Fabbiano, G., Elvis, M., et al. 2011, ApJ, 742, 23
Weaver, K. A., Mushotzky, R. F., Serlemitsos, P. J., et al. 1995, ApJ, 442, 597
Wilson, A. S., Elvis, M., Lawrence, A., & Bland-Hawthorn, J. 1992, ApJ, 391, L75
Worrall, D. M., Birkinshaw, M., O'Sullivan, E., et al. 2010, MNRAS, 408, 701

Appendix A: Spectral fits

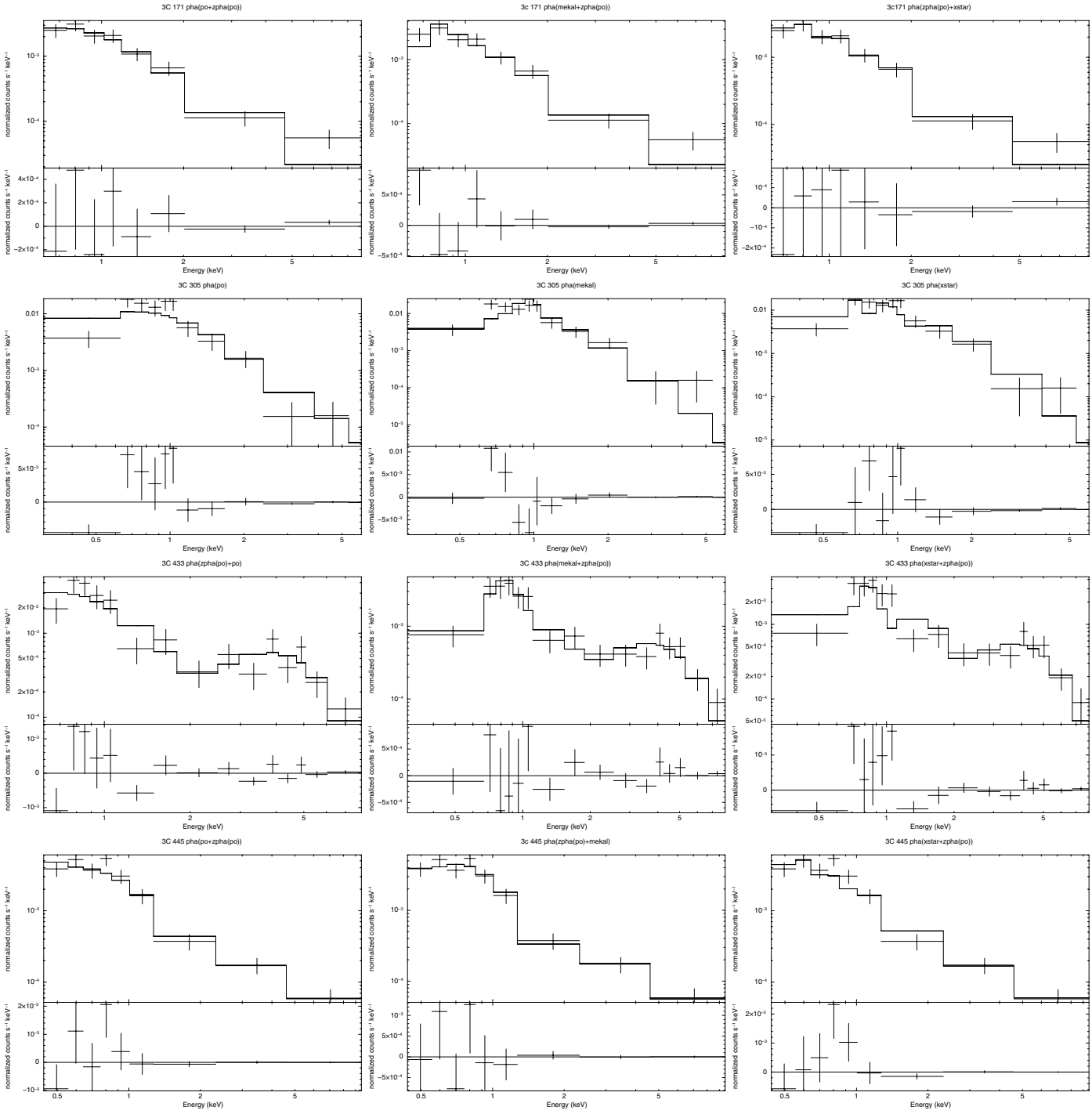

Fig. A.1. We report, as an example, the spectrum of 3C 171, 3C 305, 3C 433 and 3C 445 in the extended regions fitted with three different models: powerlaw, MEKAL, and XSTAR, absorbed by a Galactic column density value. We add to the model an intrinsically absorbed powerlaw, to reproduce the emission seen at higher energies (due to the leaking of the nuclear emission).